A deep learning-based model for characterization of atherosclerotic plaque in coronary arteries using optical coherence tomography images

Atefeh Abdolmanafi* and Luc Duong

Dept. of Software and IT Engineering,

École de technologie supérieure, Montréal, Canada

*Email:atefeh.abdolmanafi.1@ens.etsmtl.ca

Ragui Ibrahim

Div. of Cardiology, Hôpital Pierre Boucher, Longueuil, Canada

Nagib Dahdah

Div. of Pediatric Cardiology and Research Center,

Centre Hospitalier Universitaire Sainte-Justine, Montréal, Canada

(Dated: March 28, 2021)

Abstract

Purpose: Coronary artery events are mainly associated with atherosclerosis in adult population, which is recognized as accumulation of plaques in arterial wall tissues. Optical Coherence Tomography (OCT) is a light-based imaging system used in cardiology to analyze intracoronary tissue layers and pathological formations including plaque accumulation. This state-of-the-art catheter-based imaging system provides intracoronary cross-sectional images with high resolution of 10-15μm. But, interpretation of the acquired images is operator dependent, which is not only very time-consuming but also highly error prone from one observer to another. An automatic and accurate coronary plaque tagging using OCT image post-processing can contribute to wide adoption of the OCT system and reducing the diagnostic error rate.

Method: In this study, we proposed a combination of spatial pyramid pooling module with dilated convolutions for semantic segmentation to extract atherosclerotic tissues regardless of their types and training a sparse auto-encoder to reconstruct the input features and enlarge the training data as well as plaque type characterization in OCT images.

Results: The results demonstrate high precision of the proposed model with reduced computational complexity, which can be appropriate for real-time analysis of OCT images. At each step of the work, measured accuracy, sensitivity, specificity of more than 93% demonstrate high performance of the model.

Conclusion: The main focus of this study is atherosclerotic tissue characterization using OCT imaging. This contributes to wide adoption of the OCT imaging system by providing clinicians with a fully automatic interpretation of various atherosclerotic tissues. Future studies will be focused on analyzing atherosclerotic vulnerable plaques, those coronary plaques which are prone to rupture.

Keywords: Atherosclerotic plaque, Optical Coherence Tomography, Deep learning, plaque characterization

I. INTRODUCTION AND PURPOSE

Coronary artery disease (CAD) is associated with coronary atherosclerosis, which is the main leading cause of myocardial infarction with almost seven million reported deaths worldwide[1,2]. Understanding the process of plaque development, progression, and rupture is significant to guide enhancing the existing techniques for better indication of plaque morphology and improving patient's outcome. Catheter-based procedures, minimally invasive interventional methods, are prime in assisting millions of patients every year. Open heart surgery for coronary bypass intervention is therefore often avoided. Catheter-based procedures still require better understanding the type and location of coronary plaques in order to personalize treatment and target the most vulnerable lesions.

A. Atherosclerotic plaque development

Accumulation of Low-Density Lipoprotein (LDL) results in a lipid-driven coronary inflammatory called atherosclerosis. Normal arterial wall is a three-layered structure. Intima is the first arterial wall layer surrounded by endothelial cells. The second layer, media, is responsible to provide bio-mechanical strength of the artery, and control the reversible extensibility of the arterial wall during cardiac cycles. Media is composed of Smooth Muscle Cells (SMCs) and Extracellular Matrix (ECM), which is separated from intima, and the third layer, adventitia, with internal and external elastic lamina respectively. Endothelial cells provide anti-thrombotic molecules to prevent blood clot. In addition, they adjust contraction of the SMCs in Media. The inflammatory process in atherosclerosis starts with endothelial dysfunction, and accumulation of lipids in intima layer and continues by infiltration of SMCs and accumulation of macrophages to form foam cells. Progression of atherosclerotic lesions results in development of various plaque profiles including fibrous plaque, fibrocalcific plaque, fibroatheroma, and lesions with acute thrombosis[1,3]. The earliest stage of atherosclerotic plaque development is called pathological intimal thickening or fibrous plaque. Fibrous plaque is intimal thickening followed by small area of lipid pool and possible macrophage accumulation. Micro-calcification and cholesterol crystals can be seen in fibrous plaques[1,4]. Lack of enough oxygen in intimal thickening results in formation of micro-vessels with permeable and weak structure. Micro-vessels can be the sign

of plaque instability since they cause infiltration of lipids and inflammatory cells into the intima layer and followed by intraplaque haemorrhage. Intimal calcification is the most common form of fibrocalcific plaques with the lowest grade formation in fibrous plaque and the highest grade formation in fibroatheroma. Calcification is a sign of plaque stability since calcified arterial wall tissues are hard to get ruptured[1,5]. Progressive atherosclerosis is recognized by fibroatheroma development. Degrading the collagen and infiltration of SMCs results in reducing the fibrous cap thickness and remodelling of the arterial wall. Invasion of macrophages to act as mediators results in necrotic core formation. Extensive lipid pool/ necrotic core and macrophage infiltration are the most common characteristics of fibroatheroma[1,6,7]. Extensive macrophage infiltration results in plaque rupture. This leads to coronary thrombosis and acute coronary syndrome[1,8].

B. Atherosclerotic imaging

Coronary angiography (CA) is widely used in cardiology to evaluate the structural variations of coronary artery in CAD. Using x-ray, intravascular structure can be evaluated if it becomes calcified. Moreover, the system is limited to determine intracoronary plaque sub-components due to its low spatial resolution of 0.5-0.7 mm[9]. Indication of plaque morphology requires detailed information of tissues under review in cross-sectional view. Intravascular Ultrasound (IVUS) is a catheter-based imaging system, which provides gray-scale cross-sectional images of coronary artery with the resolution of 100-150 μm. IVUS is restricted to visualize plaque components due to its low spatial resolution. Virtual histology IVUS is still limited to indicate fibroatheroma, which is the most important determinant of plaque rupture[9,10]. Optical Coherence Tomography (OCT) is the state-of-the-art imaging system. OCT employs interferometry using back-scattered near-infrared light to image intracoronary cross-sections with high resolution of 10-15 μm. Due to its high resolution, OCT can provide detailed information of intracoronary tissues including plaque morphology, and plaque sub-components. Fast image acquisition, and non-ionizing radiation are other advantages of using OCT[9,11,12]. Despite the strengths, OCT has significant limitations to be addressed. Considering recent studies, Kini et al, evaluated inter-observer agreement in interpretation of OCT images. Based on this study, understanding the clinical features of various coronary plaques in OCT images can improve the inter-observer agreement in various de-

4

grees depending on the type of pathology[13]. This improved interpretation comes following extensive focused training, and yet remains sub-optimal to general practice. Considering recent studies, lack of an integrated automatic tissue characterization software system in OCT imaging for real-time high precision analysis of intracoronary tissues remains a major problem. Applying artificial intelligence paradigms will overcome the following limitation inherent to subjective operator-dependent interpretation: 1) Understanding the features of various plaques in OCT images requires intensive training, which is time-consuming for clinicians; 2) Visual interpretation of the images is still error prone compared against a trained automatic tissue characterization model; 3) Complete interpretation and manual detection of various lesions is tedious and considerably time-consuming for clinicians given the diffuse nature of coronary artery disease sequelae, which postpones the diagnostic process, decision making, and the possibility of accurate personalized treatment strategy for better patient's outcome.

II.   RELATED STUDIES

Many studies were focused on analyzing coronary artery tissues using OCT imaging. Optical properties of intracoronary tissues using OCT images were evaluated in some studies[14–19]. Other studies focused on plaque characterization using attenuation and backscattering coefficient[15]. Moreover, evaluation of coronary artery tissues as well as atherosclerotic tissue characterization were performed using various machine learning methods including combination of texture features and optical attenuation coefficients to train Random Forest as classifier[20,21] and A-line modeling for atherosclerotic plaque characterization[22].

Deep learning started to be widely used in the field of medical imaging for various applications[23–26]. Convolutional Neural Networks (CNNs) were used to classify various coronary tissues using models, which they were built and trained from scratch or applying the pre-trained models, which they can be effective by fine-tuning and transfer learning[27–30]. Deep learning-based techniques are rapidly evolving in the field of medical image analysis due to their strength in describing various tissues by considering low level to deep detailed features associated with each tissue. Such features can discriminate different tissues more precise than many other machine learning algorithms[23–26,31,32]. Patch-based classification of coronary plaques including calcium, lipid tissue, fibrous tissue, mixed tissue, and non-

5

pathological tissues were performed using CNN[33]. Another patch-based tissue classification method using VGG-based CNN was proposed to detect lipid and fibrous plaque. Training data was prepared by applying intensity based approaches as well as dilation and erosion method to remove catheter and detect lumen border[34]. Combination of four different CNN models are applied to detect vascular bifurcation using OCT imaging. Pre-processing was performed in various steps of binarization, morphological gradient, Hough transform, and cropping[35]. Macrophage accumulation was detected using normalized-intensity standard deviation approach[36]. It should be considered that macrophage accumulation results in plaque development and progression but it is not considered as coronary plaque. Also, intensity based approaches are not guaranteed to be generalized to all the cases considering very similar intensity-based features of various atherosclerotic tissues and plaques. Binary classification using a modified Resnet101-based U-net was performed to detect vulnerable plaques[37]. This study is not focused on plaque type characterization although understanding unstable plaques is important to be considered. OCT images were classified based on presence or absence of fibroatheroma. Local binary pattern, Haar-like, and histogram of oriented gradients were considered as features to train a support vector machine for binary classification and detect fibroatheroma in the images[38]. Using hand-crafted features fairly describe the intracoronary tissues, but considering the challenges of the OCT images, more detailed tissue information is required to generalize the model to all the cases. In another study, local maximum of standard deviation was used to detect lumen border as pre-processing. Then multi-layer model was proposed to classify lipid, fibrous, and calcified plaques[39]. ResNet was trained to detect lipid and calcified tissues in the work of Lee et al[40]. Pre-processing was performed in five different steps, which results in extra computational burden while using fully convolutional networks, pre-processing is not required. In the other study, pre-trained SegNet was used to detect calcification and lumen area in intracoronary OCT images[41]. In the work of Dong et al, finite element method was used for stent placement evaluation[42]. Although the focus of this study is not atherosclerotic tissue characterization, but this can be a complementary study to fully analyze coronary artery. Combination of deep and hand-crafted features were used to detect lipid and fibrocalcific plaques. Classification was performed using Random Forest[43]. In another study, combination of deep and texture features were used to train Random Forest for detection of lipid, and calcification. The usefulness of texture features should be investigated since such features are included in

6

deep features. A complete model to analyze coronary artery in OCT imaging was proposed by our team[44]. In this work, we consider the main limitations of all the related studies including our previous studies to propose a model which can overcome some limitations of
125 previous proposed methods.

III. MOTIVATION & CONTRIBUTIONS

Referring to the related studies, significant progress made to characterize various plaques in OCT imaging. We consider our previous work and other related articles to address some of their limitations and contribute in designing an atherosclerotic tissue characterization
130 model, which can be used in real-time OCT imaging. Deep learning demonstrated promising performance in the field of medical image analysis. But, there are some points regarding the deep learning models that should be considered in analyzing medical images since real-time application of these models has significant impact on accelerating the process of diagnosis and decision-making. Tuning deep learning networks for classification task results in a time-
135 consuming and complex process, which is not desirable in real-time applications. We should take the advantages of using deep learning models, but simplify the steps as much as possible. Therefore, we consider the following points in our proposed model,

- The existing studies did not focus on characterizing all the atherosclerotic plaques from early stages of the disease (development of fibrous plaque) to development of
140 fibrocalcific plaques and progression of the disease by developing lipid pool/necrotic core, which results in fibroatheroma. Also, determinant components of plaque rupture were not analyzed in the existing studies.

- To our knowledge, in all the proposed methods in the literature, various pre-processing steps were performed on the images before feeding them to the analytical model. 1.
145 Pre-processing steps are additional computational burden. 2. We may lose some important tissue information since the pre-processing steps are based on filtering and defined thresholds, which cannot be guaranteed to be generalized to all the challenging cases with high level of deformation and structural changes due to the disease.

- In most of the deep learning based existing studies, convolutional neural networks
150 (CNNs) were applied to detect few atherosclerotic plaques .CNNs demonstrate strong

features to describe various tissues in medical applications. But, using a CNN for segmentation should be patch-based, which is not efficient for various reasons including: 1) High computational burden caused by overlapped patches and redundant feature extraction. 2) Many pre-processing steps to remove unwanted information in images for reducing the computational complexity. 3) Patch-size selection is tricky considering the pooling steps in designing deep networks. 4) The input size of the network is fixed due to fully connected layers in the network architecture. Therefore, the patches should be resized.

- Lack of access to enough samples for each pathological tissue is another point to be considered in solving this problem. This is one of the reasons that patch-based CNNs were used frequently in the literature instead of using a multi-class FCNs.

This study contributes to:

- Designing a fully automatic atherosclerotic plaque characterization model to detect and characterize atherosclerotic plaques as well as pathological tissues, which are sings of plaque rupture.

- Using the original images to avoid the pre-processing steps.

- Applying spatial pyramid pooling module with dilated convolutions as a pixel-wise segmentation model overcomes many limitations of CNNs.

- Accelerating the analysis of atherosclerotic OCT images by minimizing the computational complexity, and accelerating the model performance considering advantages of using dilated convolutions instead of standard convolutions.

- Using the advantages of deep features and sparse auto-encoder to generate more features and expanding on the training data to overcome the problem of lack of enough pathological tissue samples.

- Using sparse auto-encoder for plaque type characterization with fast and accurate training using minimum feature extraction process.

This work is organized as follows: The proposed method and data collection are explained in section 4. The results are discussed in section 5, and the work is concluded in section 6.
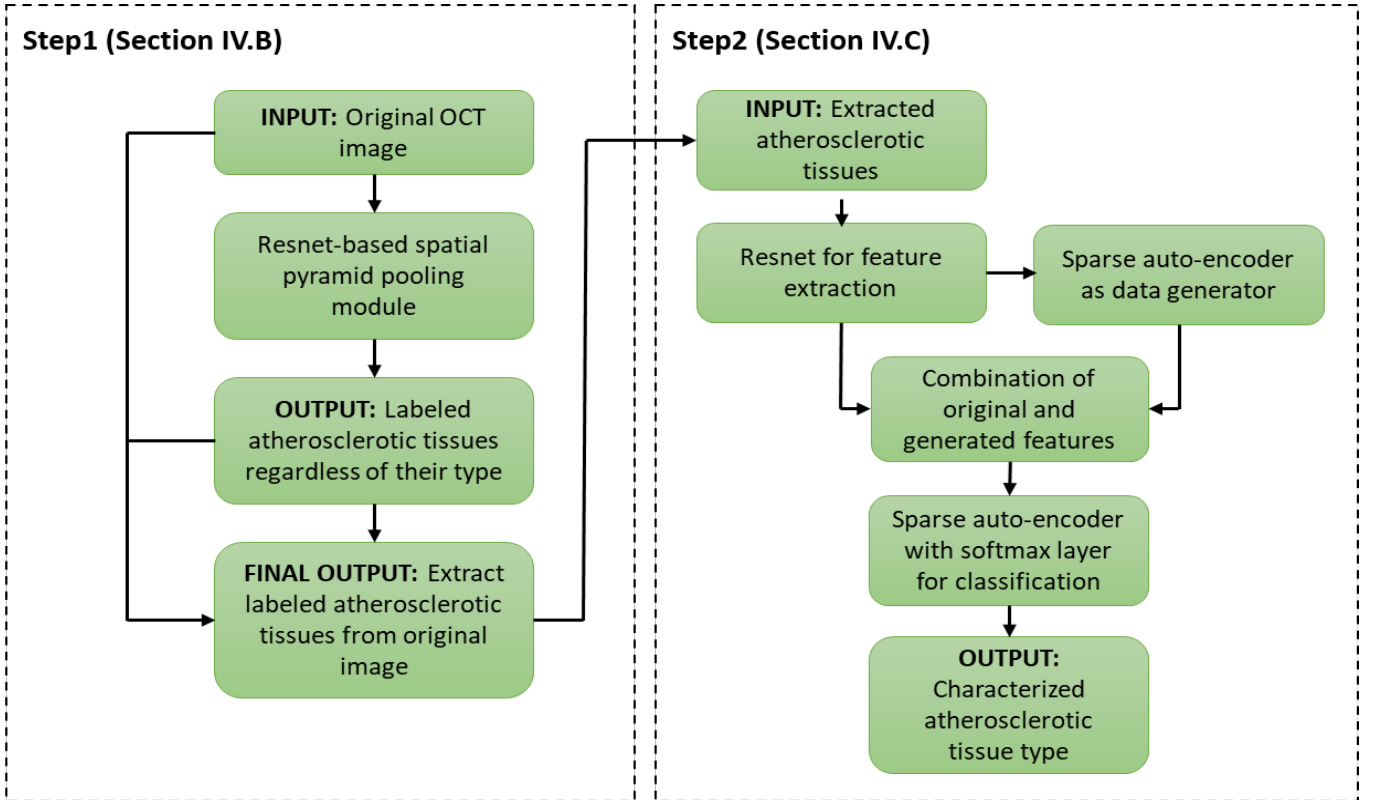
8

FIG. 1: Different steps of the atherosclerotic tissue characterization model.

IV.   MATERIAL & METHODS

¹⁸⁰   A combination of spatial pyramid pooling module with dilated convolutions is proposed for semantic segmentation to extract all atherosclerotic tissues regardless of their types in the first step. Then, sparse auto-encoders are trained on CNN features extracted from various coronary plaques and pathological formations for both feature reconstruction and plaque type characterization. The diagram of figure 1 demonstrates the workflow. When ¹⁸⁵ the network in the first step detects all the atherosclerotic tissues without considering their types, we extract them separately to feed them to the next step of the model, which is the atherosclerotic tissue type characterization. In this final step, using a Resnet as feature extractor, we extract deep feature vectors from each detected tissue in the previous step. Then, we use a sparse auto-encoder to expand on the feature map for better training our ¹⁹⁰ classifier. All the feature vectors with assigned labels for each tissue are used to train the softmax layer of the sparse auto-encoder to classify them by type. All the steps are shown in figures 1 and 2, and explained in detail in the following sections.
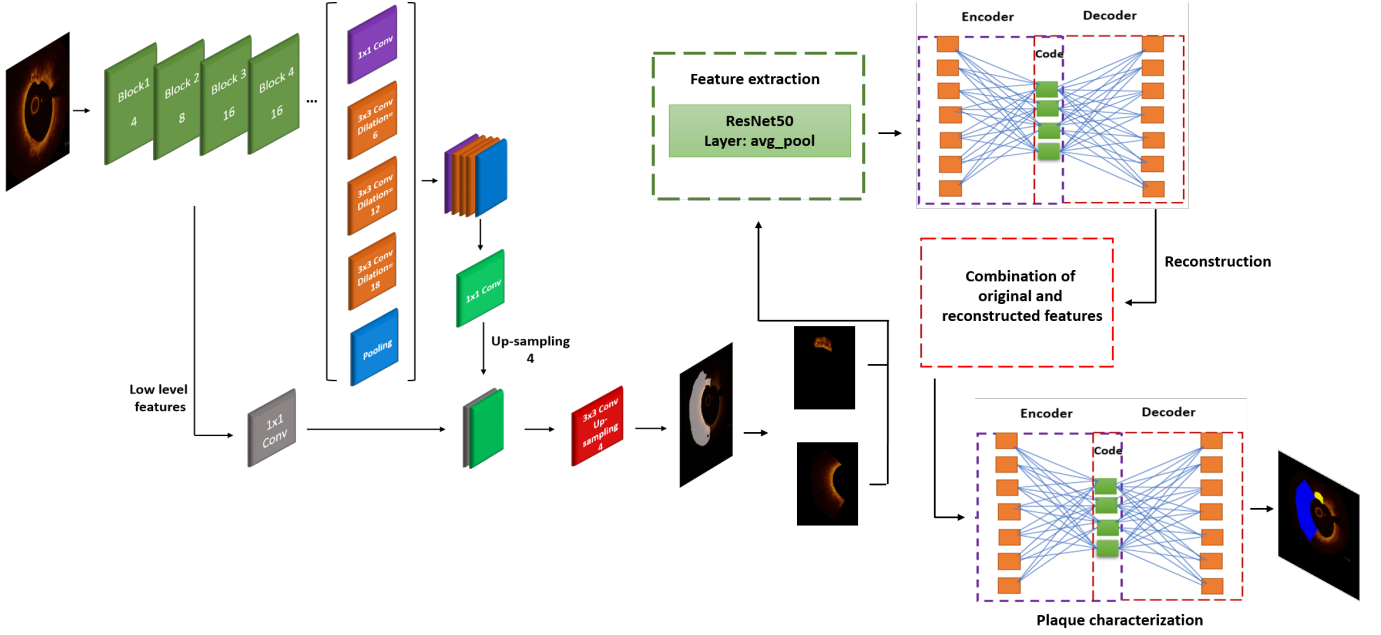
9

FIG. 2: Complete configuration of the atherosclerotic plaque characterization model consists of the following steps: 1) Resnet-based spatial pyramid pooling module with dilated convolutions for extraction of all plaques and pathological formations, 2) Feature extraction for plaque detection, 3) Sparse auto-encoder training as feature generator to expand on training data. 4) Sparse auto-encoder training to characterize various plaque types.

A. Data collection

The experiments are performed on 41 atherosclerotic OCT pullbacks. Each OCT pullback consists of approximately 200 frames of DICOM images. There are some cases with less than 200 frames per OCT pullback. Image acquisition is performed using FD-OCT (St. Jude Medical Inc., St. Paul, Minnesota, USA) with the pullback speed of 20 mm/sec. The axial and lateral resolutions of the OCT system are 12-15 μm and 20-40 μm respectively. Permission to conduct this study on retrospective OCT studies was granted by the institutional review board. We considered detecting various atherosclerotic plaques in this study including fibrous plaque, fibrocalcific plaque, fibroatheroma with lipid pool/necrotic core. We also considered miro-vessels, and thrombus since they can be assigned to plaque vulnerability. Intima is characterized as homogeneous signal-rich layer in OCT images. Media layer is visualized as a signal-poor layer with internal and external elastic lamina as signal-rich bands in OCT images. Macrophages are shown by OCT as signal-rich bright bands or
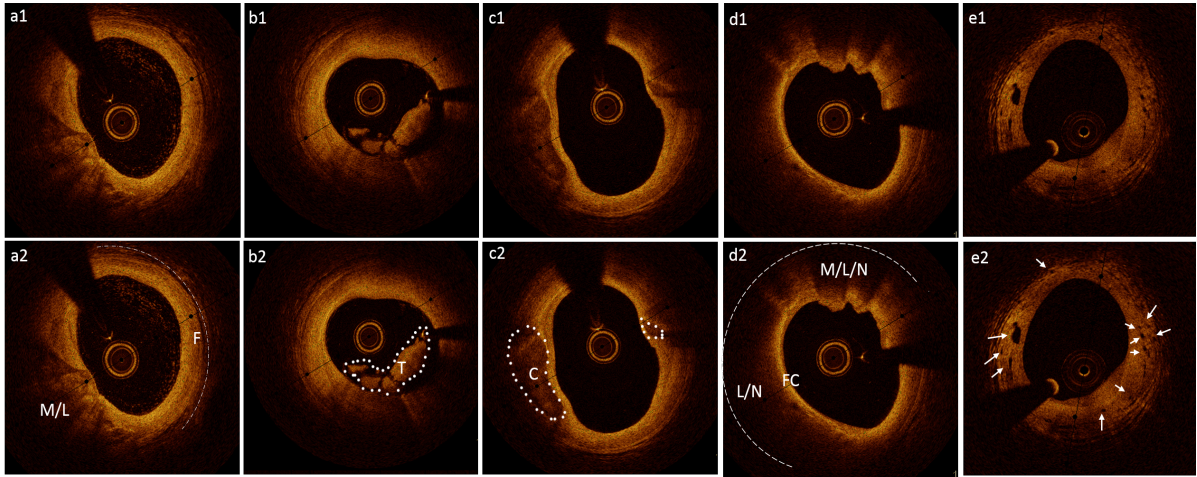
10

FIG. 3: Various atherosclerotic plaques in OCT imaging: a) a1 is the original image, and a2 is the annotated image showing fibrous plaque (F) with macrophage and lipid pool ($<$ 1 quadrant of the cross-section). b) b1 is the original image, and b2 is the annotated image showing thrombus (T) which created shadow on the arterial wall tissue. c) c1 is the original image, c2 is annotated image visualizing fibrocalcific plaque (C) and a micro-calcification. There is also macrophage accumulation with lipid pool as it is shown in the figure. d) An example of fibroatheroma with thin fibrous cap followed by macrophage accumulation and lipid pool/necrotic core. d1 represents the original image with corresponding annotated image, d2. e) An example of micro-vessel development in intimal thickening. e1 shows the original image with corresponding annotated image shown in e2. Arrows show the micro-vessels.

spots with a dorsal shadow in the direction of the light (figure 3a, 3d) and micro-vessels are visualized as rounded signal-poor structures (figure 3e). Fibrous plaque is visualized as a thick signal rich layer followed by media destruction and small area ($<$ 1 quadrant) of lipid pool and probable macrophage accumulation (figure 3a). Micro-calcification and cholesterol crystals can be seen in fibrous plaques. fibrocalcific plaque is visualized in OCT images as sharply delineated signal-poor regions (figure 3c). Necrotic core is a signal poor region, which is not distinguishable by OCT. Therefore, lipid pool/necrotic core, which takes $>$ 1 quadrant of the arterial cross-section is visualized as a signal poor region and is considered as the main characteristic of fibroatheroma (figure 3d). White and red thrombus are visualized with OCT as homogeneous signal-rich and signal-poor regions respectively (figure 3b). OCT images were labeled by trained operator using custom software in MATLAB.

Each annotated image was sent to be reviewed by two cardiologists to reach a consensus by carefully reviewing each region of interest if there is any disagreement. For atherosclerotic tissue type characterization, the total of 665 images with fibrocalcific plaque, 881 images with fibroatheroma, 204 images with thrombus, 232 images with fibrous plaque, and 70 images with micro-vessels were analyzed.

B. Extraction of atherosclerotic tissues

Different configurations of fully convolutional networks (FCNs) were used for semantic segmentation and object detection in various applications[45–48]. The models which perform spatial pyramid pooling by applying dilated convolutions demonstrated promising performances. Inspired by the study of Chen et al, employing deep convolutional neural networks with dilated convolutions results in faster and stronger encoder-decoder architecture compared against VGG-based FCN that we proposed in our previous study for extraction of various coronary pathological formations from OCT images[44,49]. We consider the advantages of both networks to develop an appropriate encoder-decoder for intracoronary OCT images. The model is built based on Resnet architecture with depthwise separable convolution structure, which is modified by using an additional parameter as dilation rate in convolutional layers as it is explained by Chen et al[49]. This network is used for semantic segmentation in the first step of our proposed model. The network is prepared for our application using fine-tuning and transfer learning to define the optimal learning parameter, and selecting the appropriate loss function, optimizer with optimal training options. Using dilated convolution results in extraction of dense feature maps, which are considerably smaller than the input resolution. This can accelerate the training process. Dilated convolutions assign an additional parameter called dilation rate to the convolutional layers. Therefore, compared against standard convolutions, the stride, number of parameters, and computational cost maintain constant while the field of view is expanded. This results in denser output feature maps, which improve the segmentation performance. Dilated convolution is applied as follows,

$$y[i] = \Sigma_k x[i + r.k]w(k) \tag{1}$$

Where i is a location in output y. Dilated convolution with dilation rate i is applied over the feature map x with kernel w. Resnet-based encoder with dilated convolutions is applied

12

in this study.

To find the optimal learning parameters, we consider extensive range of values for each parameter and evaluate the performance of the network on validation set. Assigning learning rate of 0.01 results in optimal performance of the network as it was expected considering our previous works. All the process of fine-tuning and transfer learning of pre-trained networks for the application in coronary tissue characterization using OCT imaging were explained in our previous studies[30,50]. To select the optimizer, we compare the performance of the model using both Stochastic gradient descent (Sgdm), and Adaptive moment estimation (Adam). The model performance improves by applying Adam as optimizer. Using Sgdm, the overall accuracy and the BF-score for detecting the atherosclerotic tissues are obtained as 89% and 80% respectively. While the overall accuracy and the BF-score are about 94% and 84% respectively using Adam as the optimizer. Moreover, Adam as optimizer has the advantage of requiring little memory and fast convergence. To select the appropriate loss function in this application, we evaluate the performance of the model using weighted cross-entropy, and generalized dice loss. Although the generalized dice improve the BF-score up to 83%, but the obtained overall accuracy is 70%, which is considerably lower than the obtained accuracy using weighted cross entropy. Using weighted cross entropy, both the accuracy and BF-score demonstrate the good performance of the model. Therefore, the experiments are performed by applying weighted cross entropy as the loss function. Dilation rate of 2 and 4 are applied to the last two blocks for output stride of 8 to obtain denser feature map and improve the network segmentation performance. Decoder up-samples the encoder output by up-sampling factor of 8 and combine them with corresponding low level features after applying 1x1 convolution. The last step is to refine the features using 3x3 convolutions for final segmentation result. Various atherosclerotic tissues illustrate a small fraction of the image considering the background and other surrounding tissues. Therefore, to deal with the class-imbalanced problem, we use weighted cross-entropy with the weight[51], which defined as follows,

$$w = (N - \Sigma_n p_n)/\Sigma_n p_n \qquad (2)$$

Where N is the number of images annotated as foreground with predicted probabilistic map elements p_n.

To start training the model, 80% of the images from all the pullbacks are considered as training set, and the rest 20% is divided by two to be considered as validation and test
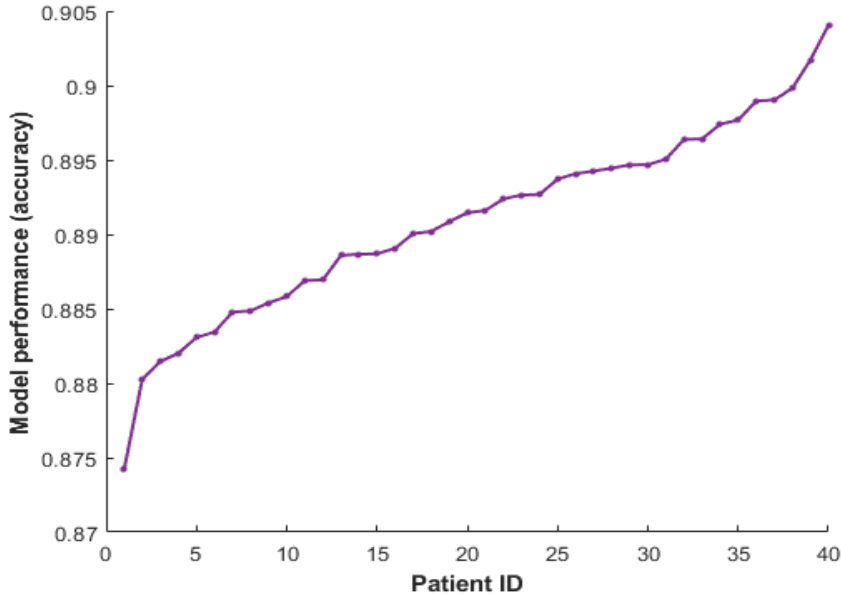
13

FIG. 4: Leave-one-out cross-validation to evaluate the performance of the first step of the model, explained in section IV.B, using various choices of training, and validation sets. It should be noted that the obtained overall accuracies in different steps of cross-validation are sorted from low to high.

sets. Leave-one-out cross-validation is performed to evaluate the performance of the model on various settings of training, validation, and test sets to assure that the model has high performance using various choices of training, and validation sets. At each step we leave one pullback as validation set, and train the model on other remaining pullbacks (figure 4).

C. Atherosclerotic tissue type characterization

The auto-encoder is a neural network with the same structure as the multi-layer perceptrons.Auto-encoders can investigate the attributes that can properly represent and reconstruct the input data. This can prevent over-fitting due to insufficient annotated data. In this study we train a sparse auto-encoder, with an additional parameter of sparsity regularization to enforce a constraint on the sparsity of the output from the hidden layer. The input data is mapped by encoder into the code, which is generated by the hidden layer. Then, decoder maps the code to reconstruct the input data. As the first step, we train the sparse auto-encoder to generate more input data. Since deep features represent detailed

14

information of the coronary tissues accurately, to accelerate the process of auto-encoder training, we apply Resnet50 as feature extractor. Since Resnet is used as feature extractor in the second step of the model, we do not need to fine-tune the network. Fine-tuning is necessary when a CNN is used as classifier. The extracted atherosclerotic tissues from the output of the first step are fed to the Resnet to extract deep feature vectors from each tissue. The features extracted from the "avg-pool" layer, right before the fully connected layer. The size of each feature vector is 2048, which results in a feature matrix with the size of 2052×2048 for all the 2052 tissue samples. All the atherosclerotic tissue types in the OCT images were annotated by trained operator. Therefore, for each feature vector extracted from each tissue, we assign the corresponding label based on our ground-truth. A detailed investigation of CNN features has been explained and visualized in our previous study[52]. The extracted deep features is used as the input data to train the sparse auto-encoder with mean square error as the loss function, L2 regularization of 0.001 with sparsity regularization, and sparsity proportion of 1 and 0.05 respectively. Training is performed for 1750 epochs. Optimal value of each parameter is selected through grid searching for various range of values by evaluating the model performance at each step of grid searching (figure 5). Satlin demonstrates the best performance as neural transfer function for both encoder and decoder. The reconstructed feature map is evaluated by measuring the mean square error between the input deep features and reconstructed features. In the second step, we combine the reconstructed features and the original features to expand on the training data for plaque type characterization. A softmax layer is trained to classify atherosclerotic plaque types including fibrous plaque, fibrocalcific plaque, and fibroatheroma and other pathological formations including micro-vessel, and thrombus since they are important factors in coronary plaque vulnerability. Then, we stack the encoder of the auto-encoder with the softmax layer to build a stacked network for classification task. It should be noted that although auto-encoder training is unsupervised, but in the second step, training the softmax layer is supervised using the training data labels. The total input data is divided into three sets of 70% for training, 15% for validation, and the remaining 15% for test. We also perform leave-one-out cross-validation to assure that the model can be generalized to all possible selections of training, validation, and test sets (figure 6).
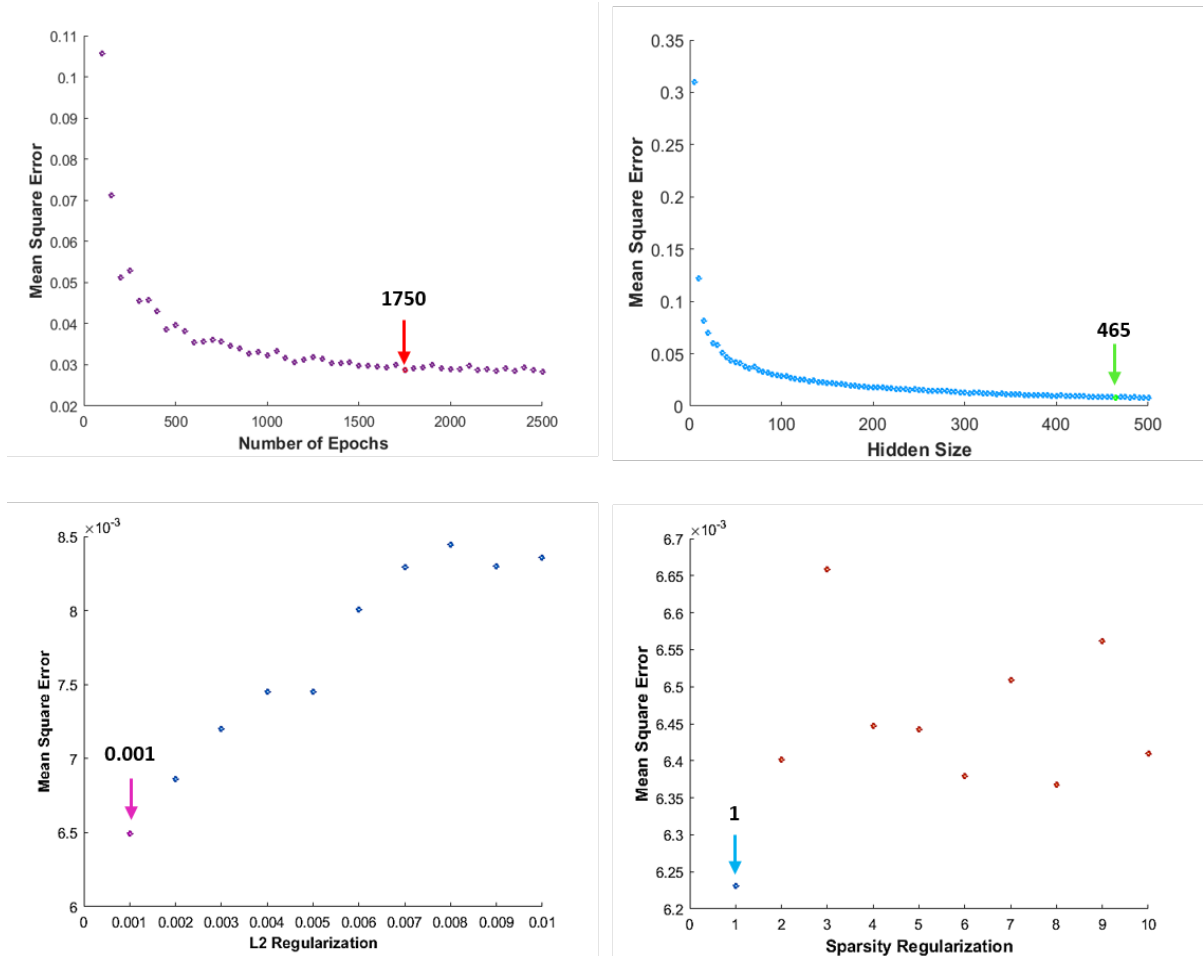
15

FIG. 5: Investigating the optimal number of epochs, hidden units, L2 regularization, and sparsity regularization to train a sparse autoencoder.

V. RESULTS & DISCUSSION

As the first step of atherosclerotic coronary analysis, all the atherosclerotic tissues including plaques and other pathological formations are extracted using a spatial pyramid pooling module with dilated convolutions to build an encoder-decoder network for foreground/background segmentation. All atherosclerotic tissues are annotated as foreground. Image background and other tissues are labeled as background. The results are shown in table I. Measured accuracy, specificity, sensitivity, and BF-score demonstrate the good performance of the model to extract all the atherosclerotic tissues regardless of their types. The training time is 29 minutes and 38 seconds for 25 epochs, the total of 2875 iterations. Mini-batch accuracy started by 42.61% for the first iteration and it reached to 97.24% at

16

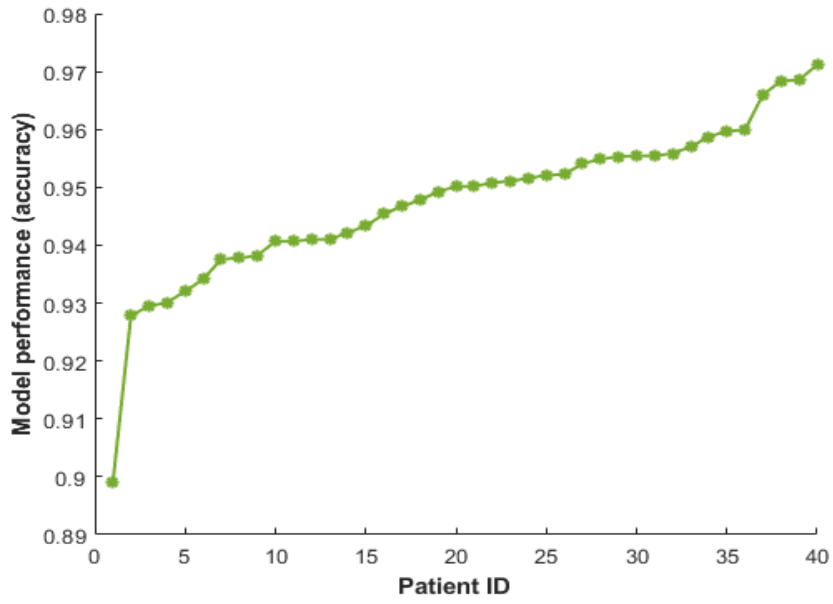FIG. 6: Leave-one-out cross-validation to evaluate the performance of the second step of the model, explained in section IV.C, to characterize tissue types using various choices of training, and validation sets. It should be noted that the obtained overall accuracies in different steps of cross-validation are sorted from low to high.
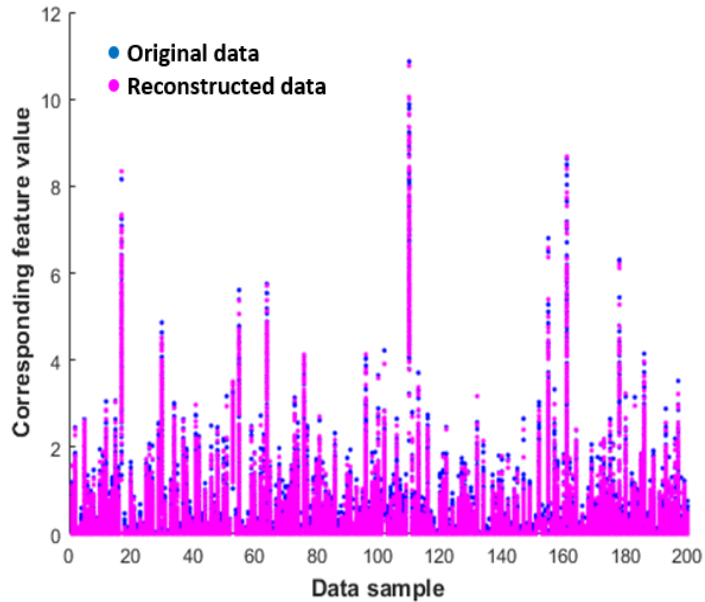

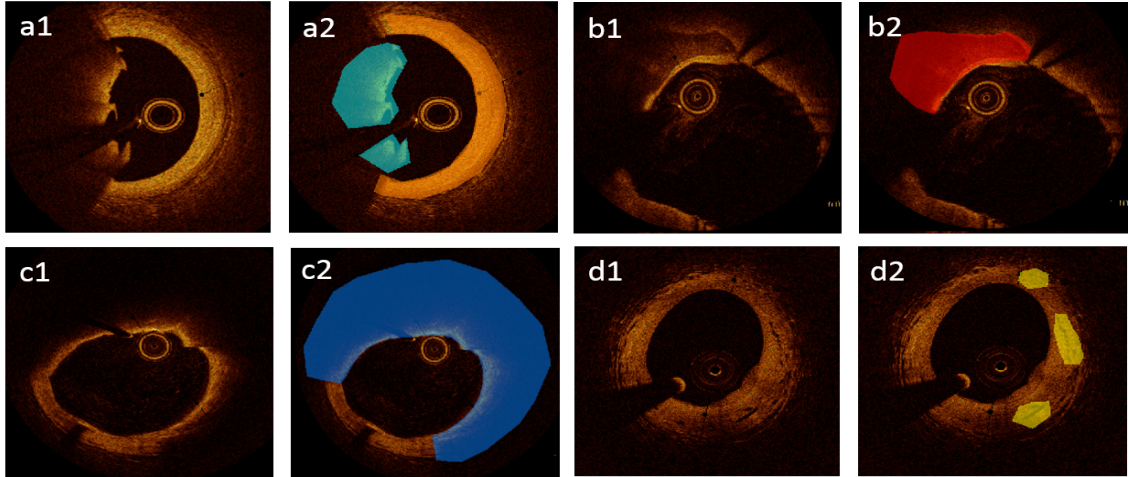FIG. 7: Overlap between the original and reconstructed features

17

FIG. 8: Atherosclerotic tissue characterization: a) a1 shows the original image, and a2 is the characterization result to detect thrombus (light blue), and fibrous plaque (orange). b) b1 is the original image, b2 is the characterization result, which detects fibrocalcific (red). c) c1 is the original image, and c2 is the result of characterization, which detects fibroatheroma with lipid pool/necrotic core. d) d1 shows the original image, and d2 is the characterization result, which shows micro-vessels (yellow)

.

the end of training. Using the trained network, automatic tissue detection for each OCT image takes approximately 0.3 seconds.

TABLE I: Measured accuracy, sensitivity, specificity, and BF-score for detecting the plaques and pathological formations regardless their types.

Tissues under review	accuracy	sensitivity	specificity	BF-Score
Atherosclerotic tissues	0.93 ± 0.10	0.90 ± 0.13	0.95 ± 0.07	0.84 ± 0.18

The next step is to train the sparse auto-encoders for two reasons: 1)Feature reconstruction, 2) Atherosclerotic tissue type characterization. Using deep features, training the auto-encoder is very fast with accurate performance. We use deep features extracted from various plaques as input of the sparse auto-encoder. The mean square error measured between the original input features and reconstructed features is 0.006. The overlap between the original and reconstructed features is shown in figure 7 for small portion of the data. For plaque classification including fibrous plaque, fibrocalcific, and fibroatheroma as well as

18

Confusion Matrix

FIG. 9: Confusion matrix related to the atherosclerotic tissue type characterization: Labels 1 to 5 represent fibrous plaque, thrombus, fibrocalcific, micro-vessel, and fibroatheroma, respectively. The rows represent the classifier output, and the columns represent the true classes according to the ground-truth. The diagonal cells represent the samples which are correctly classified. The column on the right side represents per-class precision, and the row at the bottom of the confusion matrix represents the per-class sensitivity.

.

other pathological formations such as thrombus and micro-vessel, a softmax layer is trained in 1000 epochs. Per-class classification results shown in table II and figure 9 demonstrate the high performance of the model. The final classification model assigns a label from the range of 1 to 5 to the various atherosclerotic tissues in an OCT image. Based on the predicted label, the corresponding tissue will be shown with a color code in the original OCT image. This is how the classification result of the auto-encoder can be converted into the visual representation of the result. Visual representation of the proposed atherosclerotic tissue characterization model is shown in figure 8.

As it was mentioned previously in this article, the models we propose in the field of

TABLE II: Measured accuracy, sensitivity, specificity, for plaque type characterization

Atherosclerotic tissues	accuracy	sensitivity	specificity
Fibrous plaque	0.96	0.94	0.99
Fibrocalcific	0.99	0.98	0.99
Fibroatheroma	0.99	0.99	0.99
Thrombus	0.98	0.97	0.99
Micro-vessel	0.90	0.80	1.00

medical image analysis are designed to be applicable in real-time analysis of tissues under review. Therefore, not only the models should perform precisely, but also they should be fast with reduced computational complexity as much as possible. In this particular problem, we considered the following points in designing our model:

- Using the interventional imaging systems, it is preferred to avoid interventions as much as possible for patient's safety. Therefore, there is lack of enough data to start from scratch in designing a deep learning-based model. To overcome this issue, we use pre-trained networks since the architectures were validated on very large datasets and can be transferred to be used for our application with different choices of parameters, loss function, optimizer, and training options. But designing an appropriate and precise model based on these pre-trained networks highly depends on accurate investigation of the problem and the tissues under review.

- Pathological tissues have different types, and they develop in various stages of the disease.Therefore, in some segments of the imaged artery, we may not have any plaque, or we may have one type, which is more common (fibrous plaque in early stages of the disease or fibroatheroma in disease progression). For other plaques or pathological tissues, they develop or not in different stages of the disease. Therefore, the number of developed pathological tissues varies from one patient to another and depends on many factors such as the level of disease progression, and the specific tissue texture and functionality in each patient. This results in accessing to limited number of pathological tissues in our analyses, which can affect the training process.

- In technical point of view, our segmentation model has good performance if it can

20

capture various aspects of the segmentation quality. Therefore, high rate of correctly labeled pixels and good contour segmentation are both important to be considered in evaluation of our model performance. To this end, not only the accuracy, sensitivity, and specificity are important to be measured to evaluate the number of correctly labeled pixels, but also, BF-score is important to have high value since it is the measure of a good contour segmentation.

Considering all the above points, we applied the spatial pyramid pooling with dilated convolution in two different ways: 1. Multi-class segmentation to detect all types of atherosclerotic tissues: In this case, the accuracy, sensitivity, and specificity demonstrated fair values, but the BF-score of less than 60% demonstrated poor performance of the model. Therefore, our overall evaluation for model performance was not satisfying in addressing our problem in this study. The visual representation of the result verifies the noisy result using this approach. Also, random selection of the training set is not possible in this approach since we had to control our training set to assure that it has been taught with all the atherosclerotic tissue types. 2. Foreground/background segmentation to detect all atherosclerotic tissues regardless of their types: In this approach, all the evaluation metrics (accuracy, sensitivity, specificity, and BF-score) demonstrate high performance of the model for both correctly labeled pixels, and contour segmentation (table I).

For tissue type characterization, we improved our previous study by addressing its limitations. In our previous work, we tried to reduce the computational burden while we kept the model precision high. But, there are some limitations regarding our previous model that we address in this study: 1) Our previous model was proposed for intracoronary tissue characterization in pediatric patients affected by Kawasaki disease. The model we propose in this study considers the atherosclerotic tissues. Therefore, plaque types and clinical features of atherosclerotic tissues should be considered in designing our new intracoronary tissue characterization algorithm. 2) In our previous model, we extracted all the lesions and plaques regardless of their types using a VGG-based FCN, which worked properly. In this study, we had to modify the model not only to be adapted to atherosclerotic tissues, but also to reduce the computational complexity as well. Therefore, we employed the advantage of using dilated convolutions in this step of the work. 3) For tissue type characterization using our previous model, we applied three CNNs to extract three different sets of feature maps to train Random Forest to discriminate between various tissues. Then, majority voting

21

approach was applied to all the three sets of classifier decisions to deliver the final decision. This method is efficient considering fast and accurate performance of CNNs as feature extractors to train other classifiers with less complexity, which Random Forest worked better than other classifiers in our application. But, using three different CNNs result in three different sets of deep feature matrices, and three times training of the Random Forest. The whole process takes less time than fine-tuning and training a deep learning model as a classifier, but we could significantly reduce the computational complexity even more than our previous model by employing sparse auto-encoders and using only one set of deep features while the results show the high precision of the model.

We also considered the limitations of the existing studies to design our proposed model. Therefore, the efficiency of the proposed model is not only because of the details of the network architecture, but it is more about the selection of the networks and the way we solved the problem to address the limitations of the existing studies. For this purpose, we considered the following points:

- In the field of OCT image analysis, we deal with tissues at a very small scale. Every pixel is important to be considered in our analysis since the region of interest is very small. Therefore, we should select a mathematical model which can consider all the tissue information, deformation and pathological changes caused by disease.

- Lack of large datasets and lack of enough samples for each pathological formation is another point to be considered in designing our model.

- The aim of this study is to accelerate, facilitate, and improve the diagnostic process by designing a model which can analyze atherosclerotic tissues precisely. Therefore, we should consider the model, which is not computationally expensive while it has high precision in detecting the plaques and pathological tissues.

Considering the existing studies, to our knowledge, pre-processing was performed prior to feeding the images to the proposed analytical model. Not only the pre-processing steps are additional computational burden, but also they are based on defining various filtering and thresholds, which cannot be guaranteed to be generalized to all the cases specifically when we have considerable deformation and structural changes due to the disease. In more detail, When a network was trained on the original images without any pre-processing: 1) The

22

network understands the original image as the input image. Therefore, when the trained network is used in clinical application, no pre-processing is required, and the network can get the original image as the input and in less than a second (0.3 seconds) return the result with detected atherosclerotic tissues. But, if the pre-processing steps apply on the original images prior to feeding them to the network, the trained network only understands the pre-processed image as the input. Therefore, when the model is used in clinical applications, the pre-processing steps should be performed on the original images and make the images recognizable for the network as input. This results in more computation time due to pre-processing steps. 2) Secondly, considering the unpredictable deformations of the artery due to the disease, we may face some cases during the analysis that designed pre-processing steps result in losing important tissue information if they cannot be applicable properly on that specific case. Therefore, it is safe and more accurate if we avoid the pre-processing steps.

Since we used the original images without pre-processing, we had to consider the networks, which can keep using the original images while it performs fast and accurate to analyze the images. Therefore, using patch based convolutional neural networks for segmentation, which was proposed in many existing studies cannot be efficient. The reason is that feeding the original image without any pre-processing to a CNN results in a very time-consuming and expensive computational process. The patches are overlapped, and this results in redundant feature extraction and classification. Choosing the patch size, which can match the kernel size of each convolutional layer is very challenging. Also, the input size of the CNNs is fixed because of the fully connected layers in their architecture. Therefore, we cannot use the original size of the images and we have to resize the patches to the acceptable input size of the network. Therefore, we decided to use a fully convolutional network, which the input size can be flexible based on our application. Pixel to pixel segmentation using encoder-decoder is fast even if the original images are fed to the network. Also, using dilated convolutions instead of standard convolution can contribute to maintaining the same number of parameters as standard convolution but accelerate and accurate the analysis based on the defined dilation rate. To deal with the problem of lack of access to large datasets, we fine-tuned the pre-trained networks by defining the hyper-parameters and the loss function, which are more appropriate for our application. Also, to deal with the problem of lack of enough samples for each pathological tissues to train the FCN for multi-class segmentation, we divided our analytical process into two different steps: 1. Extracting all the plaques

and pathological tissues regardless of their types using a FCN, and train an auto-encoder to classify them by type.

TABLE III: Inter-observer agreement for fibrous tissue

Observers	Observer1	Observer2	Ground-truth	Model
Observer1	1.00	0.45	0.51	0.53
Observer2		1.00	0.58	0.58
Ground-truth			1.00	0.98
Model				1.00

TABLE IV: Inter-observer agreement for calcification

Observers	Observer1	Observer2	Ground-truth	Model
Observer1	1.00	0.77	0.85	0.85
Observer2		1.00	0.84	0.84
Ground-truth			1.00	0.98
Model				1.00

TABLE V: Inter-observer agreement for fibroatheroma

Observers	Observer1	Observer2	Ground-truth	Model
Observer1	1.00	0.68	0.56	0.53
Observer2		1.00	0.62	0.58
Ground-truth			1.00	0.95
Model				1.00

We asked two observers to interpret the images, the inter-observer reliability was measured by calculating the confusion matrix between every two observers for each tissue type separately. The inter-observed agreement is reported in the following tables for each tissue type separately. The same calculations were performed for each observer interpretation versus ground-truth as well as the tissue characterization model. The reported results in tables III-VII show the disagreement between the observers in visual recognition of challenging tissue types (fibrous and fibroatheroma) while in less challenging tissue type recognition the

24

TABLE VI: Inter-observer agreement for micro-vessel

Observers	Observer1	Observer2	Ground-truth	Model
Observer1	1.00	0.82	0.92	0.90
Observer2		1.00	0.88	0.88
Ground-truth			1.00	0.96
Model				1.00

TABLE VII: Inter-observer agreement for thrombus

Observers	Observer1	Observer2	Ground-truth	Model
Observer1	1.00	0.89	0.90	0.88
Observer2		1.00	0.97	0.97
Ground-truth			1.00	0.98
Model				1.00

inter-observer agreement is high. This demonstrates the necessity of having access to an automatic system to characterize various atherosclerotic tissue types. The agreement between ground-truth and the model decision for all the tissue types demonstrates the robustness of the model performance based on what it was trained for to recognize and characterize. Briefly, this investigation demonstrates two important points: 1. Superiority of the system compared against human observation, and 2. Different levels of difficulties for individual readers depending on the type of lesions. More precisely, our proposed end-to-end pipeline to detect and characterize atherosclerotic tissues can overcome the following limitations inherent to subjective operator-dependent interpretation:

- Understanding the features of various plaques in OCT images requires intensive training, which is time-consuming for clinicians.

- Visual interpretation of the images is still error prone compared against a trained automatic tissue characterization model.

- complete interpretation and manual detection of various lesions may take weeks and even months for clinicians given the diffuse nature of coronary artery disease sequelae, which postpones the diagnostic process, decision making, and the possibility of accurate personalized treatment strategy for better patient's outcome.

Using the trained network, automatic tissue detection for each OCT image takes approximately 0.3 seconds. Depends on the size of the arterial wall segment, which is studied using OCT imaging, tissue detection for an OCT pullback including around 200 images will take about 60 seconds. Therefore, analyzing and studying OCT pullbacks obtained from 100 patients takes less than 2 hours. With human intervention, the interpretation of the images for 100 patients can take over weeks and even months. Therefore, the automatic segmentation model can considerably accelerate the identification time.

In this study, we detect some significant determinants of plaque vulnerability such as micro-vessels, thrombus, and fibroatheroma with macrophage infiltration and lipid pool/necrotic core formation. This can be the base of our future work to design a model, which can only analyze plaque vulnerability.

VI. CONCLUSION

This study is focused on atherosclerotic tissue characterization using OCT imaging. This can contribute to wide adoption of OCT imaging system by providing clinicians with fully automatic interpretation of various atherosclerotic tissues. Our proposed model composed of an encoder-decoder with dilated convolutions to extract all atherosclerotic tissues regardless their type. Then, training sparse autoencoders on deep features for either feature reconstruction and atherosclerotic tissue type characterization. For future work, we mainly focus on analyzing plaque vulnerability in more details than our current study.

VII. CONFLICTS OF INTEREST

The authors declare no conflicts of interest.

VIII. FUNDING

This study is supported by BoBeau Coeur—Fondation CHU Ste-Justine in Montreal.

* Email: atefeh.abdolmanafi.1@ens.etsmtl.ca; Atefeh Abdolmanafi

[1] L. S. Lilly, *Pathophysiology of heart disease: a collaborative project of medical students and faculty* (Lippincott Williams & Wilkins, 2012).

[2] R. Pahwa and I. Jialal, *Atherosclerosis. statpearls. treasure island (fl)* (2018).

[3] J. E. Wagenseil and R. P. Mecham, Journal of cardiovascular translational research **5**, 264 (2012).

[4] F. Otsuka, M. Joner, F. Prati, R. Virmani, and J. Narula, Nature Reviews Cardiology **11**, 379 (2014).

[5] T. Saita, K. Fujii, H. Hao, T. Imanaka, M. Shibuya, M. Fukunaga, K. Miki, H. Tamaru, T. Horimatsu, M. Nishimura, et al., European Heart Journal-Cardiovascular Imaging **18**, 342 (2017).

[6] P. K. Cheruvu, A. V. Finn, C. Gardner, J. Caplan, J. Goldstein, G. W. Stone, R. Virmani, and J. E. Muller, Journal of the American College of Cardiology **50**, 940 (2007).

[7] K. Yahagi, F. D. Kolodgie, F. Otsuka, A. V. Finn, H. R. Davis, M. Joner, and R. Virmani, Nature Reviews Cardiology **13**, 79 (2016).

[8] K. Yahagi, H. R. Davis, E. Arbustini, and R. Virmani, Atherosclerosis **239**, 260 (2015).

[9] J. M. Tarkin, M. R. Dweck, N. R. Evans, R. A. Takx, A. J. Brown, A. Tawakol, Z. A. Fayad, and J. H. Rudd, Circulation research **118**, 750 (2016).

[10] A. Erglis, S. Jegere, and I. Narbute, Interventional Cardiology Review **9**, 151 (2014).

[11] M. W. Lee, J. W. Song, W. J. Kang, H. S. Nam, T. S. Kim, S. Kim, W.-Y. Oh, J. W. Kim, and H. Yoo, Scientific reports **8**, 1 (2018).

[12] B. E. Bouma, M. Villiger, K. Otsuka, and W.-Y. Oh, Biomedical optics express **8**, 2660 (2017).

[13] A. S. Kini, Y. Vengrenyuk, T. Yoshimura, M. Matsumura, J. Pena, U. Baber, P. Moreno, R. Mehran, A. Maehara, S. Sharma, et al., Journal of the American College of Cardiology **69**, 644 (2017).

[14] J. Schmitt, A. Knüttel, and R. Bonner, Applied Optics **32**, 6032 (1993).

[15] J. M. Schmitt, A. Knuttel, M. Yadlowsky, and M. Eckhaus, Physics in Medicine & Biology **39**, 1705 (1994).

[16] C. Xu, J. M. Schmitt, S. G. Carlier, and R. Virmani, Journal of biomedical optics **13**, 034003 (2008).

[17] G. Van Soest, T. P. Goderie, E. Regar, S. Koljenovic, A. G. J. van Leenders, N. Gonzalo, S. van Noorden, T. Okamura, B. E. Bouma, G. J. Tearney, et al., Journal of biomedical optics **15**,

27

545   011105 (2010).

[18] K. Vermeer, J. Mo, J. Weda, H. Lemij, and J. De Boer, Biomedical optics express **5**, 322 (2014).

[19] S. Liu, Y. Sotomi, J. Eggermont, G. Nakazawa, S. Torii, T. Ijichi, Y. Onuma, P. W. Serruys, B. P. Lelieveldt, and J. Dijkstra, Journal of biomedical optics **22**, 096004 (2017).

[20] G. J. Ughi, T. Adriaenssens, P. Sinnaeve, W. Desmet, and J. D'hooge, Biomedical optics express **4**, 1014 (2013).

[21] L. S. Athanasiou, C. V. Bourantas, G. Rigas, A. I. Sakellarios, T. P. Exarchos, P. K. Siogkas, A. Ricciardi, K. K. Naka, M. I. Papafaklis, L. K. Michalis, et al., Journal of biomedical optics **19**, 026009 (2014).

[22] J. J. Rico-Jimenez, D. U. Campos-Delgado, M. Villiger, K. Otsuka, B. E. Bouma, and J. A. Jo, Biomedical optics express **7**, 4069 (2016).

[23] M. Biswas, V. Kuppili, D. R. Edla, H. S. Suri, L. Saba, R. T. Marinho, J. M. Sanches, and J. S. Suri, Computer methods and programs in biomedicine **155**, 165 (2018).

[24] Y. Dong, Y. Pan, X. Zhao, R. Li, C. Yuan, and W. Xu, in *Smart Computing (SMARTCOMP), 2017 IEEE International Conference on* (IEEE, 2017), pp. 1–8.

[25] K. Lekadir, A. Galimzianova, À. Betriu, M. del Mar Vila, L. Igual, D. L. Rubin, E. Fernández, P. Radeva, and S. Napel, IEEE J. Biomedical and Health Informatics **21**, 48 (2017).

[26] R.-M. Menchón-Lara, J.-L. Sancho-Gómez, and A. Bueno-Crespo, Applied Soft Computing **49**, 616 (2016).

[27] G. Litjens, T. Kooi, B. E. Bejnordi, A. A. A. Setio, F. Ciompi, M. Ghafoorian, J. A. Van Der Laak, B. Van Ginneken, and C. I. Sánchez, Medical image analysis **42**, 60 (2017).

[28] S. He, J. Zheng, A. Maehara, G. Mintz, D. Tang, M. Anastasio, and H. Li, in *Medical Imaging 2018: Image Processing* (International Society for Optics and Photonics, 2018), vol. 10574, p. 1057432.

[29] C. Kolluru, D. Prabhu, Y. Gharaibeh, H. Bezerra, G. Guagliumi, and D. Wilson, Journal of Medical Imaging **5**, 044504 (2018).

[30] A. Abdolmanafi, L. Duong, N. Dahdah, and F. Cheriet, Biomedical optics express **8**, 1203 (2017).

[31] A. Fourcade and R. Khonsari, Journal of stomatology, oral and maxillofacial surgery **120**, 279 (2019).

[32] D. Shen, G. Wu, and H.-I. Suk, Annual review of biomedical engineering **19**, 221 (2017).

28

³³ L. S. Athanasiou, M. L. Olender, M. José, E. Ben-Assa, and E. R. Edelman, in *Medical Imaging 2019: Computer-Aided Diagnosis* (International Society for Optics and Photonics, 2019), vol. 10950, p. 109500N.

³⁴ X. Ren, H. Wu, Q. Chen, T. Kubo, and T. Akasaka, in *International Forum on Medical Imaging in Asia 2019* (International Society for Optics and Photonics, 2019), vol. 11050, p. 1105015.

³⁵ M. Miyagawa, M. G. F. Costa, M. A. Gutierrez, J. P. G. F. Costa, and C. F. F. Costa Filho, Ieee Access **7**, 66167 (2019).

³⁶ J. J. Rico-Jimenez, D. U. Campos-Delgado, L. M. Buja, D. Vela, and J. A. Jo, Atherosclerosis **290**, 94 (2019).

³⁷ L. Li and T. Jia, Reviews in cardiovascular medicine **20**, 171 (2019).

³⁸ Q. Yan, M. Xu, D. W. K. Wong, A. Taruya, A. Tanaka, J. Liu, P. Wong, and J. Cheng, Journal of Ambient Intelligence and Humanized Computing pp. 1–7 (2019).

³⁹ X. Ren, H. Wu, Q. Chen, T. Imai, T. Kubo, and T. Akasaka, IEICE Transactions on Information and Systems **102**, 2238 (2019).

⁴⁰ J. Lee, D. Prabhu, C. Kolluru, Y. Gharaibeh, V. N. Zimin, H. G. Bezerra, and D. L. Wilson, Biomedical Optics Express **10**, 6497 (2019).

⁴¹ Y. Gharaibeh, D. Prabhu, C. Kolluru, J. Lee, V. Zimin, H. Bezerra, and D. Wilson, Journal of Medical Imaging **6**, 045002 (2019).

⁴² P. Dong, H. Mozafari, D. Prabhu, H. G. Bezerra, D. L. Wilson, and L. Gu, Journal of Biomechanical Engineering **142** (2020).

⁴³ J. Lee, D. Prabhu, C. Kolluru, Y. Gharaibeh, V. N. Zimin, L. A. Dallan, H. G. Bezerra, and D. L. Wilson, Scientific reports **10**, 1 (2020).

⁴⁴ A. Abdolmanafi, F. Cheriet, L. Duong, R. Ibrahim, and N. Dahdah, Journal of biophotonics **13**, e201900112 (2020).

⁴⁵ R. Mottaghi, X. Chen, X. Liu, N.-G. Cho, S.-W. Lee, S. Fidler, R. Urtasun, and A. Yuille, in *Proceedings of the IEEE Conference on Computer Vision and Pattern Recognition* (2014), pp. 891–898.

⁴⁶ M. Cordts, M. Omran, S. Ramos, T. Rehfeld, M. Enzweiler, R. Benenson, U. Franke, S. Roth, and B. Schiele, in *Proceedings of the IEEE conference on computer vision and pattern recognition* (2016), pp. 3213–3223.

⁴⁷ B. Zhou, H. Zhao, X. Puig, S. Fidler, A. Barriuso, and A. Torralba, in *Proceedings of the IEEE*

conference on computer vision and pattern recognition (2017), pp. 633–641.

[48] H. Caesar, J. Uijlings, and V. Ferrari, in *Proceedings of the IEEE Conference on Computer Vision and Pattern Recognition* (2018), pp. 1209–1218.

[49] L.-C. Chen, Y. Zhu, G. Papandreou, F. Schroff, and H. Adam, in *Proceedings of the European conference on computer vision (ECCV)* (2018), pp. 801–818.

[50] A. Abdolmanafi, L. Duong, N. Dahdah, I. R. Adib, and F. Cheriet, Biomedical Optics Express **9**, 4936 (2018).

[51] C. H. Sudre, W. Li, T. Vercauteren, S. Ourselin, and M. J. Cardoso, in *Deep Learning in Medical Image Analysis and Multimodal Learning for Clinical Decision Support* (Springer, 2017), pp. 240–248.

[52] A. Abdolmanafi, L. Duong, N. Dahdah, and F. Cheriet, IEEE journal of biomedical and health informatics **23**, 931 (2018).